

# Detection of weak maneuvering target based on keystone transform and matched filtering process

Zhi Sun, Xiaolong Li, Wei Yi\*, Guolong Cui, Lingjiang Kong

School of Electronic Engineering, University of Electronic Science and Technology of China, Chengdu, Sichuan 611731, PR China



## ARTICLE INFO

### Article history:

Received 10 January 2017

Revised 5 April 2017

Accepted 11 May 2017

Available online 12 May 2017

### Keywords:

Weak maneuvering target

Range migration

Doppler frequency migration

Keystone transform

Matched filtering process

## ABSTRACT

Detection of weak maneuvering target often suffers from the problems of the range migration (RM) and the Doppler frequency migration (DFM) within the coherent pulse interval. In order to eliminate the RM and DFM, a new coherent integration method based on keystone transform (KT) and matched filtering process (MFP), i.e., KT-MFP, is proposed. Specifically, this method firstly corrects the linear RM caused by the unambiguous velocity via KT and then the MFP, which jointly searching in the fold factor and acceleration domain, is carried out to remove the residual RM and compensate the DFM. At last, coherent integration of the target's energy is achieved through the slow time Fourier transform (FT). The advantage of the proposed method is that it can obtain superior coherent integration and detection performance for both the slow-moving and fast-moving target, in comparison with the existing algorithms. In addition, KT-MFP could avoid the blind speed sidelobe (BSSL) effect. Numerical simulations are performed to assess the performance from different aspects, i.e., computational complexity, coherent integration for a low-speed target, detection performance for a low-speed target, coherent integration for a high-speed target, detection performance for a high-speed target and coherent integration for multi-targets.

© 2017 Elsevier B.V. All rights reserved.

## 1. Introduction

With the great progress of science and technology, maneuvering target detection has drawn more and more attention in modern radar field [1–9]. In general, there exists the problem of the weak radar returns because of the low radar cross section (RCS) of the maneuvering targets, which may make the detection more difficult [10–13]. Increasing the integration time can improve the detection performance effectively with the help of coherent integration technique [14,15]. Unfortunately, the conventional detection method, e.g. moving target detection (MTD) algorithm, might be confronted with a performance loss because of the range migration (RM) and the Doppler frequency migration (DFM) caused by the complex motions (i.e., velocity and acceleration) of maneuvering targets during the long coherent integration time [16–21]. In order to solve the problems of RM and DFM, several methods are introduced as follows.

The keystone transform (KT), which can eliminate the linear RM effectively through rescaling the time axis, is one of the most popular methods [22–25]. Radon Fourier transform (RFT) is another method which can integrate the energy via searching along the directions of range and velocity [26,27]. However, the coherent in-

tegration methods mentioned above may suffer a serious performance loss as long as the DFM effect appears.

In order to compensate the DFM and achieve the coherent integration, an efficient method based on KT and fractional Fourier transform (FRFT), i.e., KT-FRFT, was proposed [28]. Another method combining the improved axis rotation (IAR) and FRFT, named as IAR-FRFT, was employed to realize the coherent integration for the target with a constant acceleration [29]. The KT-FRFT or IAR-FRFT could correct the linear RM induced by the target's velocity via KT or IAR. After that, the DFM compensation and coherent integration can be obtained by FRFT. Nevertheless, these two methods could not correct the quadratic RM caused by the target's acceleration which would lead to a performance loss. The generalized Radon Fourier transform (GRFT) was then presented to remove the quadratic RM and DFM and complete the coherent integration [26,30]. Particularly, GRFT can achieve the coherent integration by jointly searching along the target trajectory. Although GRFT could obtain a good detection performance, it often suffers a huge computational burden. Moreover, due to the discrete pulse sampling, limited range resolution and finite integration time [31], the blind speed sidelobe (BSSL) effect would inevitably appear in the GRFT output, which might bring about severe false alarm and the detection performance loss [30].

In this paper, for the sake of removing the RM (including the linear RM and the quadratic RM) and DFM to achieve the coherent

\* Corresponding author.

E-mail address: [kussoyi@gmail.com](mailto:kussoyi@gmail.com) (W. Yi).

integration, a method based on KT and matched filtering process (MFP), i.e., KT-MFP, is presented. In particular, KT is performed to correct the linear RM induced by the unambiguous velocity at first. Then, the MFP, via jointly searching in the fold factor and acceleration domain, is conducted to eliminate the residual linear RM caused by the blind velocity as well as the quadratic RM and DFM effect resulted from the acceleration. In the end, the slow time Fourier transform (FT) is performed to achieve the coherent integration.

Generally speaking, the presented method can obtain not only the superior coherent integration but also the better detection performance both for the low-speed target and high-speed target, in compared with RFT, IAR-FRFT and KT-FRFT. Additionally, the KT-MFP method has lower computational complexity than GRFT and could avoid the BSSL effect. Eventually, numerical experiments are performed to verify the effectiveness of the proposed method.

The remaining sections of this paper are organized as follows. In Section 2, the signal model is established. Then the proposed coherent integration method, i.e., KT-MFP, is given in Section 3. Besides, we analyze the coherent integration for multi-targets as well as the computational complexity of KT-MFP and GRFT in this section. In Section 4, we evaluate the performance via several numerical experiments from several aspects, including coherent integration for a low-speed target, detection performance for a low-speed target, coherent integration for a high-speed target, detection performance for a high-speed target and coherent integration for multiple targets. At last, we make a conclusion in Section 5.

## 2. Signal model and problem formulation

Consider that the pulse Doppler (PD) radar transmits a narrow-band linear frequency modulated (LFM) signal with the mathematical model as follow [32,33]

$$s(\tau, t_m) = \text{rect}\left(\frac{\tau}{T_p}\right) \exp(j\pi\gamma\tau^2) \exp[j2\pi f_c(\tau + t_m)], \quad (1)$$

where

$$\text{rect}\left(\frac{\tau}{T_p}\right) = \begin{cases} 1 & |\tau| \leq T_p/2, \\ 0 & |\tau| > T_p/2, \end{cases}$$

$\exp(\cdot)$  is the exponential function [26,27,30].  $\tau$  denotes the fast time and  $t_m = mT$  is the slow time,  $m = 0, 1, 2, \dots, M-1$ .  $M$  represents the total integration pulse number of radar and  $T$  indicates the pulse repetition interval.  $T_p$  and  $f_c$  denote the pulse duration and the carrier frequency, respectively.  $\gamma = \frac{B}{T_p}$  is the frequency modulated rate and  $B$  is the signal bandwidth.

Ignoring the high order components and supposing that the instantaneous slant range between the radar and a moving target with an acceleration satisfies [29,34–38]

$$r(t_m) = r_0 + a_1 t_m + a_2 t_m^2, \quad (2)$$

where  $r_0$  is the initial slant range between the radar and the target,  $a_1$  and  $a_2$  denote the radial velocity and acceleration, respectively.

Assume  $|a_1| \ll c$  ( $c$  denotes the speed of light) and then the received baseband echo signal after the demodulation can be expressed as [39,40]

$$s_r(\tau, t_m) = A_0 \text{rect}\left(\frac{\tau - \beta}{T_p}\right) \exp\left(-j\frac{4\pi r(t_m)}{\lambda}\right) \times \exp[j\pi\gamma(\tau - \beta)^2] \exp\left(-j\frac{4\pi a_1 t_m}{\lambda}\right), \quad (3)$$

where  $A_0$  is the target reflectance,  $\lambda = \frac{c}{f_c}$  represents the radar wavelength,  $\beta = \frac{2r(t_m)}{c}$  is the delay time.

Then, we can use the matched filter, i.e.,  $h(\tau) = \text{rect}\left(\frac{\tau}{T_p}\right) \exp(j\pi\gamma\tau^2)$ , to realize the pulse compression (PC)

and the compressed signal in the range frequency-slow time  $(f - t_m)$  domain may be written as [5]

$$S_c(f, t_m) = A_1 \text{rect}\left(\frac{f + f_d/2}{B - f_d}\right) \exp\left(-j\frac{\pi f_d^2}{\gamma}\right) \times \exp\left[-j\frac{4\pi(f + f_c + f_d)r(t_m)}{c}\right], \quad (4)$$

where  $A_1 = A_0 \times \sqrt{D}$  denotes the complex amplitude of the signal echoes after PC and  $D = B \times T_p$  is the pulse compression ratio [10].  $f_d = \frac{2a_1}{\lambda}$  is the Doppler frequency.

Because of target's high-speed and the low pulse repetition frequency (PRF) of radar, the velocity may exceed the value of PRF, which will bring about the velocity ambiguity effect [41]. So the velocity  $a_1$  satisfies

$$a_1 = ka_{amb} + a_0, \quad (5)$$

where  $a_{amb} = \frac{\lambda \text{PRF}}{2}$  is the blind velocity,  $k$  is the fold factor,  $a_0$  denotes the unambiguous velocity with the range of  $[-a_{amb}/2, a_{amb}/2]$  [42].

Substituting (2) and (5) into (4) yields

$$S_c(f, t_m) = A_2 \exp\left[-j\frac{4\pi(f + f_c + f_d)r_0}{c}\right] \times \exp\left[-j\frac{4\pi(f + f_c + f_d)a_0 t_m}{c}\right] \times \exp\left[-j\frac{4\pi(f + f_c + f_d)a_2 t_m^2}{c}\right] \times \exp\left[-j\frac{4\pi(f + f_c + f_d)ka_{amb} t_m}{c}\right], \quad (6)$$

where  $A_2 = A_1 \text{rect}\left(\frac{f + f_d/2}{B - f_d}\right) \exp\left(-j\frac{\pi f_d^2}{\gamma}\right)$ . Ignoring the effect of  $f_d$ , (6) can be expressed as follow [5,6]

$$S_c(f, t_m) = A_2 \exp\left[-j\frac{4\pi(f + f_c)r_0}{c}\right] \times \exp\left[-j\frac{4\pi(f + f_c)a_0 t_m}{c}\right] \times \exp\left[-j\frac{4\pi(f + f_c)a_2 t_m^2}{c}\right] \times \exp\left(-j\frac{4\pi f k a_{amb} t_m}{c}\right) \times \exp(-j2\pi \text{PRF} k t_m). \quad (7)$$

It should be pointed out that  $\exp(-j2\pi \text{PRF} k t_m) = 1$  [5,31]. So (7) can be rewritten as

$$S_c(f, t_m) = A_2 \exp\left[-j\frac{4\pi(f + f_c)r_0}{c}\right] \times \exp\left[-j\frac{4\pi(f + f_c)a_0 t_m}{c}\right] \times \exp\left[-j\frac{4\pi(f + f_c)a_2 t_m^2}{c}\right] \times \exp\left(-j\frac{4\pi f k a_{amb} t_m}{c}\right). \quad (8)$$

Clearly, the last three exponential terms of (8) are all coupling terms with respect to slow-time  $t_m$  and range-frequency  $f$ . In particular,

- $\exp[-j\frac{4\pi(f+f_c)a_0t_m}{c}]$  denotes the term of unambiguous velocity, which will cause the linear RM.
- $\exp(-j\frac{4\pi f k a_{amb} t_m}{c})$  represents the term of blind velocity, which would also result in the linear RM.
- $\exp[-j\frac{4\pi(f+f_c)a_2t_m^2}{c}]$  may bring about the quadratic RM and DFM which can make the integration energy dispersed.

In order to solve the problems of RM and DFM and obtain the coherent accumulation, KT-MFP is proposed in the following section.

### 3. Coherent integration via KT-MFP

In this section, the detailed processes of the proposed method, i.e., KT-MFP, are introduced. Furthermore, the coherent integration via the KT-MFP for the multi-targets is also analyzed. Finally, the KT-MFP method is also compared with GRFT in terms of the computational complexity.

#### 3.1. Keystone transform

Firstly, apply KT, which is performed as  $t_m = \frac{f_c}{f+f_c} t_n$  ( $t_n$  is the new slow-time variable), to eliminate the linear range migration [22,23,25]. Then (8) can be represented in the  $f - t_n$  domain as

$$S_{KT}(f, t_n) = A_2 \exp \left[ -j \frac{4\pi(f+f_c)r_0}{c} \right] \times \exp \left( -j \frac{4\pi a_0 t_n}{\lambda} \right) \times \exp \left[ -j \frac{4\pi k a_{amb} t_n f}{\lambda(f+f_c)} \right] \times \exp \left[ -j \frac{4\pi a_2 t_n^2 f_c}{\lambda(f+f_c)} \right]. \quad (9)$$

Consider that the radar transmits a narrowband signal, the range-frequency variable  $f$  satisfies  $f \ll f_c$ , so  $\frac{f_c}{f+f_c} \approx 1 - \frac{f}{f_c}$  and  $f + f_c \approx \frac{f_c^2}{f_c - f}$  [43]. Thus (9) can be recast as

$$S_{KT}(f, t_n) = A_2 \exp \left[ -j \frac{4\pi(f+f_c)r_0}{c} \right] \times \exp \left( -j \frac{4\pi a_0 t_n}{\lambda} \right) \times \exp \left[ -j \frac{4\pi k a_{amb} t_n f (f_c - f)}{c f_c} \right] \times \exp \left[ -j \frac{4\pi a_2 t_n^2 (f_c - f)}{c} \right]. \quad (10)$$

Through the second exponential term in (10), it can be seen that the linear RM resulted from unambiguous velocity  $a_0$  has been corrected. However, the last two exponential terms indicate that the linear RM caused by the blind velocity and the quadratic RM induced by acceleration still exist.

#### 3.2. Matched filtering process

To eliminate the residual RM and the DFM in (10), we define the matched filtering function as

$$H_m(f, t_n; k', a'_2) = \exp \left[ j \frac{4\pi k' a_{amb} t_n f (f_c - f)}{c f_c} \right] \times \exp \left[ j \frac{4\pi a'_2 t_n^2 (f_c - f)}{c} \right], \quad (11)$$

where  $k'$  is the searching fold factor and  $a'_2$  denotes the searching acceleration. Multiplying (11) by (10) yields

$$S_{KT}(f, t_n; k', a'_2) = A_2 \exp \left[ -j \frac{4\pi(f+f_c)r_0}{c} \right] \times \exp \left( -j \frac{4\pi a_0 t_n}{\lambda} \right) \times \exp \left[ j \frac{4\pi(k' - k)a_{amb} t_n f (f_c - f)}{c f_c} \right] \times \exp \left[ j \frac{4\pi(a'_2 - a_2)t_n^2 (f_c - f)}{c} \right]. \quad (12)$$

When  $k' = k$  and  $a'_2 = a_2$ , namely, the searching fold factor and the acceleration are matched with the target's fold factor and acceleration, respectively. Therefore, (12) can be rewritten as

$$S_{match}(f, t_n) = A_2 \exp \left[ -j \frac{4\pi(f+f_c)r_0}{c} \right] \times \exp \left( -j \frac{4\pi a_0 t_n}{\lambda} \right). \quad (13)$$

From (13), one can see that the residual RM caused by the blind velocity and the acceleration can be removed. Besides, the DFM effect resulted from the acceleration could also be compensated. After the RM and DFM compensation via KT and MFP, applying the range IFT to (13), we can get

$$S_{match}(\tau, t_n) = A_3 \text{sinc} \left[ B \left( \tau - \frac{2r_0}{c} \right) \right] \exp \left( -j \frac{4\pi r_0}{\lambda} \right) \times \exp \left( -j \frac{4\pi a_0 t_n}{\lambda} \right), \quad (14)$$

where  $\text{sinc}(x) = \frac{\sin \pi x}{\pi x}$  is the sinc function [11,30]. In addition,  $A_3 = A_2 G_r$  denotes the complex amplitude (after the range IFT) and  $G_r$  is the compression gain for range IFT. Finally, performing the slow time FT on (14), we can achieve the coherent integration, i.e.,

$$S_{int}(\tau, f_{t_n}) = A_5 \text{sinc} \left[ B \left( \tau - \frac{2r_0}{c} \right) \right] \text{sinc} \left[ CPI \left( f_{t_n} + \frac{2a_0}{\lambda} \right) \right], \quad (15)$$

where  $A_5 = A_4 \exp \left( -j \frac{4\pi r_0}{\lambda} \right)$ . Furthermore,  $A_4 = A_3 G_s$  is the integration amplitude (after the slow time FT) and  $G_s$  indicates the compression gain of the slow time FT. Additionally,  $CPI = MT$  represents the coherent processing interval while  $f_{t_n}$  is the Doppler frequency with respect to  $t_n$ .

From (14) and (15), we can see that the coherent integration reaches its maximum value when the searching fold factor  $k'$  and acceleration  $a'_2$  are precisely matched. Thus the estimated function of  $k$  and  $a_2$ , i.e.,  $(\hat{k}, \hat{a}_2)$ , can be achieved as follow

$$(\hat{k}, \hat{a}_2) = \arg \max_{(k', a'_2)} | \text{FT}_{f_{t_n}} \{ \text{IFT}_{f} \{ S_{KT}(f, t_n) \times H_m(f, t_n; k', a'_2) \} \} |. \quad (16)$$

where  $\text{IFT}_f(\cdot)$  and  $\text{FT}_{f_{t_n}}(\cdot)$  indicate, respectively, the IFT over the range frequency variable  $f$  and the FT with respect to the slow time variable  $t_n$ .

According to the peak location of (15), we could also obtain the value of the Doppler frequency  $f_{t_n}$ , which has the relationship with unambiguous velocity as  $a_0 = -\frac{\lambda f_{t_n}}{2}$ . Then the estimation value of  $\hat{a}_0$  can be written as

$$\hat{a}_0 = -\frac{\lambda}{2} \arg \max_{f_{t_n}} | \text{FT}_{f_{t_n}} \{ \text{IFT}_f \{ S_{KT}(f, t_n) H_m(f, t_n; k', a'_2) \} \} |. \quad (17)$$

Thereby, we can achieve the value of  $\hat{a}_1$ , which indicates the estimated velocity, as follow

$$\hat{a}_1 = \hat{a}_0 + \hat{k} a_{amb}. \quad (18)$$

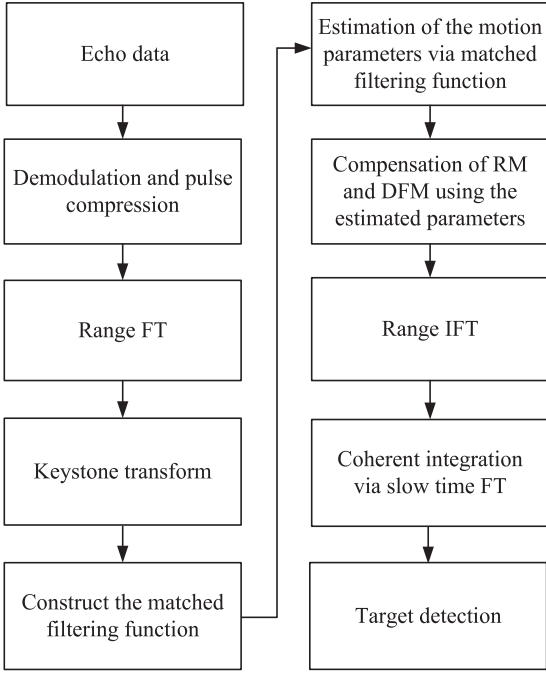


Fig. 1. Flow chart of KT-MFP.

One can see that the coherent integration of target's energy can be obtained from (15). On condition that the peak value of (15) exceeds the given threshold, the target could be detected. It should be noted that the searching scopes of  $k'$  and  $a'_2$  are  $[k'_{\min}, k'_{\max}]$  and  $[a'_{2\min}, a'_{2\max}]$ , where the searching intervals are  $\Delta k' = f_c/(Mf_s)$  ( $f_s$  denotes the sampling rate) [5] and  $\Delta a'_2 = \lambda/(2CPI^2)$  [11], respectively. Additionally, the summarized framework of the proposed method is given in **Algorithm 1** while the flowchart is shown in Fig. 1.

### 3.3. KT-MFP for multi-targets

Assume that there are  $L$  targets in the scene. Without loss of generality, the derivation of KT-MFP for the  $l$ th target is given in the following. The instantaneous slant range of the  $l$ th target with complex motions satisfies [29,30,34]

$$r_l(t_m) = r_{0l} + a_{1l}t_m + a_{2l}t_m^2, \quad (19)$$

where  $r_{0l}$  is the initial slant range from the radar to the  $l$ th target,  $a_{1l}$  and  $a_{2l}$  respectively indicate the  $l$ th target's radial velocity and acceleration.

Note that the velocity of the  $l$ th target could be written as follow

$$a_{1l} = k_l a_{amb} + a_{0l}, \quad (20)$$

where  $k_l$  and  $a_{0l}$  represent the fold factor and the unambiguous velocity of the  $l$ th target, respectively.

Furthermore, the received signal after PC could be expressed as [20,44]

$$S_{mc}(f, t_m) = \sum_{l=1}^L A_{1l} \text{rect}\left(\frac{f + f_{dl}/2}{B - f_{dl}}\right) \exp\left(-j\frac{\pi f_{dl}^2}{\gamma}\right) \times \exp\left[-j\frac{4\pi(f + f_c + f_{dl})r_l(t_m)}{c}\right], \quad (21)$$

where  $A_{1l}$  is the complex amplitude of the  $l$ th target after PC,  $f_{dl}$  denotes the  $l$ th target's Doppler frequency.

**Algorithm 1:** Summarize: the main procedures of the KT-MFP method.

```

1 Input: raw data  $s_r(\tau, t_m)$ , searching scopes, i.e.,  $[k'_{\min}, k'_{\max}]$  and  $[a'_{2\min}, a'_{2\max}]$ .
2 Pulse compression: Perform PC on  $s_r(\tau, t_m)$ , then apply the FT along the  $\tau$  to obtain the compressed signal  $S_c(f, t_m)$  by (4).
3 Keystone transform: Apply KT on  $S_c(f, t_m)$  and obtain  $S_{KT}(f, t_n)$  through (9).
4 Matched filtering process: Go through each  $k'$  in  $[k'_{\min}, k'_{\max}]$  with the interval  $\Delta k'$  and  $a'_2$  in  $[a'_{2\min}, a'_{2\max}]$  with the interval  $\Delta a'_2$ .
5 for  $k' = k'_{\min}, \dots, k'_{\max}$  do
6   for  $a'_2 = a'_{2\min}, \dots, a'_{2\max}$  do
7     Multiply the matched filtering function  $H_m(f, t_n; k', a'_2)$  and  $S_{KT}(f, t_n)$  to obtain  $S_{KT}(f, t_n; k', a'_2)$  via (12);
8     Apply the range IFT and the slow time FT on  $S_{KT}(f, t_n; k', a'_2)$ ;
9     Preserve the peak value of  $S_{KT}(f, t_n; k', a'_2)$ ;
10   end
11 end
12 Find the maximal peak value, then the corresponding  $k'$  and  $a'_2$  are the estimated fold factor  $\hat{k}$  and acceleration  $\hat{a}_2$ .
13 Output:  $(\hat{k}, \hat{a}_2)$ .
14 Coherent integration: Using  $(\hat{k}, \hat{a}_2)$  to compensate  $S_{KT}(f, t_n)$  into  $S_{match}(f, t_n)$  by (13). Perform the range IFT and the slow time FT on  $S_{match}(f, t_n)$ , then one can achieve the coherent integration  $s_{int}(\tau, t_n)$  through (15).
  
```

Ignoring the effect of  $f_{dl}$ , then substituting (19) and (20) into (21) yields

$$S_{mc}(f, t_m) = \sum_{l=1}^L A_{2l} \exp\left[-j\frac{4\pi(f + f_c)r_{0l}}{c}\right] \times \exp\left[-j\frac{4\pi(f + f_c)a_{0l}t_m}{c}\right] \times \exp\left[-j\frac{4\pi(f + f_c)a_{2l}t_m^2}{c}\right] \times \exp\left(-j\frac{4\pi f_k a_{amb} t_m}{c}\right). \quad (22)$$

where  $A_{2l} = A_{1l} \text{rect}\left(\frac{f + f_{dl}/2}{B - f_{dl}}\right) \exp\left(-j\frac{\pi f_{dl}^2}{\gamma}\right)$ . It should also be noted that  $\exp(-j2\pi PRF_k t_m) = 1$  in the above equation.

Then, performing KT on (22), we have

$$S_{mKT}(f, t_n) = \sum_{l=1}^L A_{2l} \exp\left[-j\frac{4\pi(f + f_c)r_{0l}}{c}\right] \times \exp\left(-j\frac{4\pi a_{0l}t_n}{\lambda}\right) \times \exp\left[-j\frac{4\pi k_l a_{amb} t_n f}{\lambda(f + f_c)}\right] \times \exp\left[-j\frac{4\pi a_{2l}t_n^2 f}{\lambda(f + f_c)}\right]. \quad (23)$$

Similarly, since the radar transmits a narrowband signal ( $f \ll f_c$ ), thus we still have  $\frac{f_c}{f + f_c} \approx 1 - \frac{f}{f_c}$  and  $f + f_c \approx \frac{f_c^2}{f_c - f}$ , so (23) could be

reconstructed as

$$\begin{aligned} S_{\text{mKT}}(f, t_n) &= \sum_{l=1}^L A_{2l} \exp \left[ -j \frac{4\pi(f + f_c)r_{0l}}{c} \right] \\ &\times \exp \left( -j \frac{4\pi a_{0l}t_n}{\lambda} \right) \\ &\times \exp \left[ -j \frac{4\pi k_l a_{\text{amb}}t_n f(f_c - f)}{c f_c} \right] \\ &\times \exp \left[ -j \frac{4\pi a_{2l}t_n^2(f_c - f)}{c} \right]. \end{aligned} \quad (24)$$

Next, we define the matched filtering function for the  $l$ th target as

$$\begin{aligned} H_{\text{mul}}(f, t_n; k_l', a_{2l}') &= \exp \left[ j \frac{4\pi k_l' a_{\text{amb}}t_n f(f_c - f)}{c f_c} \right] \\ &\times \exp \left[ j \frac{4\pi a_{2l}' t_n^2(f_c - f)}{c} \right], \end{aligned} \quad (25)$$

where  $k_l'$  represents the searching fold factor of the  $l$ th target and  $a_{2l}'$  is the  $l$ th target's searching acceleration. Multiplying (25) by (24), we can get

$$\begin{aligned} S_{\text{mKT}}(f, t_n; k_l', a_{2l}') &= \sum_{l=1}^L A_{2l} \exp \left[ -j \frac{4\pi(f + f_c)r_{0l}}{c} \right] \\ &\times \exp \left( -j \frac{4\pi a_{0l}t_n}{\lambda} \right) \\ &\times \exp \left[ j \frac{4\pi(k_l' - k_l)a_{\text{amb}}t_n f(f_c - f)}{c f_c} \right] \\ &\times \exp \left[ j \frac{4\pi(a_{2l}' - a_{2l})t_n^2(f_c - f)}{c} \right]. \end{aligned} \quad (26)$$

When  $k_l' = k_l$  and  $a_{2l}' = a_{2l}$ , i.e., the searching fold factor and searching acceleration are respectively equal to the  $l$ th target's fold factor and acceleration. Then (26) could be recast as

$$\begin{aligned} S_{\text{mul}}(f, t_n) &= A_{2l} \exp \left[ -j \frac{4\pi(f + f_c)r_{0l}}{c} \right] \\ &\times \exp \left( -j \frac{4\pi a_{0l}t_n}{\lambda} \right) + S_{\text{other}}(f, t_n). \end{aligned} \quad (27)$$

where

$$\begin{aligned} S_{\text{other}}(f, t_n) &= \sum_{g=1, g \neq l}^L A_{2g} \exp \left[ -j \frac{4\pi(f + f_c)r_{0g}}{c} \right] \\ &\times \exp \left( -j \frac{4\pi a_{0g}t_n}{\lambda} \right) \\ &\times \exp \left[ j \frac{4\pi(k_g' - k_l)a_{\text{amb}}t_n f(f_c - f)}{c f_c} \right] \\ &\times \exp \left[ j \frac{4\pi(a_{2g}' - a_{2l})t_n^2(f_c - f)}{c} \right]. \end{aligned} \quad (28)$$

From (27), we can see that the RM and DFM of the  $l$ th target are both corrected. By conducting the range IFT and the slow time FT on (27), we have

$$\begin{aligned} s_{\text{mint}}(\tau, f_{t_n}) &= A_{5l} \text{sinc} \left[ B \left( \tau - \frac{2r_{0l}}{c} \right) \right] \\ &\times \text{sinc} \left[ \text{CPI} \left( f_{t_n} + \frac{2a_{0l}}{\lambda} \right) \right] + S_{\text{other}}(\tau, f_{t_n}), \end{aligned} \quad (29)$$

where

$$S_{\text{other}}(\tau, f_{t_n}) = \text{FT}_{t_n} \left[ f \text{IFT}(S_{\text{other}}(f, t_n)) \right] \quad (30)$$

**Table 1**  
Computational complexity of GRFT and KT-MFP.

Methods	Multiplications	Additions
GRFT	$MNN_{a_1}N_{a_2}$	$(M-1)NN_{a_1}N_{a_2}$
KT-MFP	$MN \log_2 N/2$ $+(M^2 + 2M)N$ $+N_k N_{a_2} MN \log_2 M/2$	$MN \log_2 N$ $+(M+2N)(M-1)$ $+N_k N_{a_2} MN \log_2 M$

**Table 2**  
Simulation parameters of radar for the low-speed target.

Carrier frequency $f_c$	2.4 GHz
Bandwidth $B$	40 MHz
Sample frequency $f_s$	60 MHz
Pulse repetition frequency $PRF$	1500 Hz
Pulse duration $T_p$	1 us
Number of pulses $M$	900

**Table 3**  
Simulation parameters of radar for the high-speed target.

Carrier frequency $f_c$	10 GHz
Bandwidth $B$	1 MHz
Sample frequency $f_s$	5 MHz
Pulse repetition frequency $PRF$	200 Hz
Pulse duration $T_p$	100 us
Number of pulses $M$	201

$A_{5l} = A_{2l} G_{rl} G_{sl} \exp \left( -j \frac{4\pi r_{0l}}{\lambda} \right)$  denotes the integration amplitude. Moreover,  $G_{rl}$  is the compression gain for the range IFT and  $G_{sl}$  indicates the compression gain of the slow time FT.

**Remark.** Note that the KT is a linear transform and could simultaneously correct the effect of the linear RM induced by the unambiguous velocity. In addition, the MFP is also a linear procedure. Therefore, there is no cross-talk among the multi-targets. Moreover, it should be pointed out that the KT-MFP method could obtain the coherent integration for multiple targets simultaneously when the scattering intensities of the targets are approximately equal. However, if the scattering intensities of different targets are strikingly different, the weak targets may be shadowed by the strong ones and the coherent integration will become difficult for the weak targets. Then, the CLEAN technique [44–46] could be applied to eliminate the effect of the strong targets and highlight the weak ones. By this way, the coherent integration of the strong and weak targets can be achieved iteratively [44–46].

### 3.4. Computational complexity

In what follows, we analyze the computational complexity of the major steps in GRFT [30] and the proposed method. As far as the arithmetic types, the complex multiplication and addition operations are presented. We define the number of searching range cells, echo pulses, searching velocity, searching acceleration and searching fold factor as  $N, M, N_{a_1}, N_{a_2}, N_k$ , respectively. In terms of the KT-MFP method, the KT operation needs  $MN \log_2 N/2 + (M^2 + 2M)N$  multiplications and  $MN \log_2 N + (M+2N)(M-1)$  additions to correct the linear RM caused by the unambiguous velocity. When we perform the MFP to eliminate the residual RM and the DFM,  $N_k N_{a_2} MN \log_2 M/2$  and  $N_k N_{a_2} MN \log_2 M$  are necessary. While GRFT method needs  $MNN_{a_1}N_{a_2}$  multiplications and  $(M-1)NN_{a_1}N_{a_2}$  additions [30]. The detailed computational complexity of GRFT and KT-MFP is listed in Table 1. Then, using respectively the parameters of the radar in Table 2 (for the low-speed target) and Table 3 (for the high-speed target), we can achieve the ratio of the computational complexity between GRFT and KT-MFP (which varying with the pulse number), as shown in Fig. 2. In par-

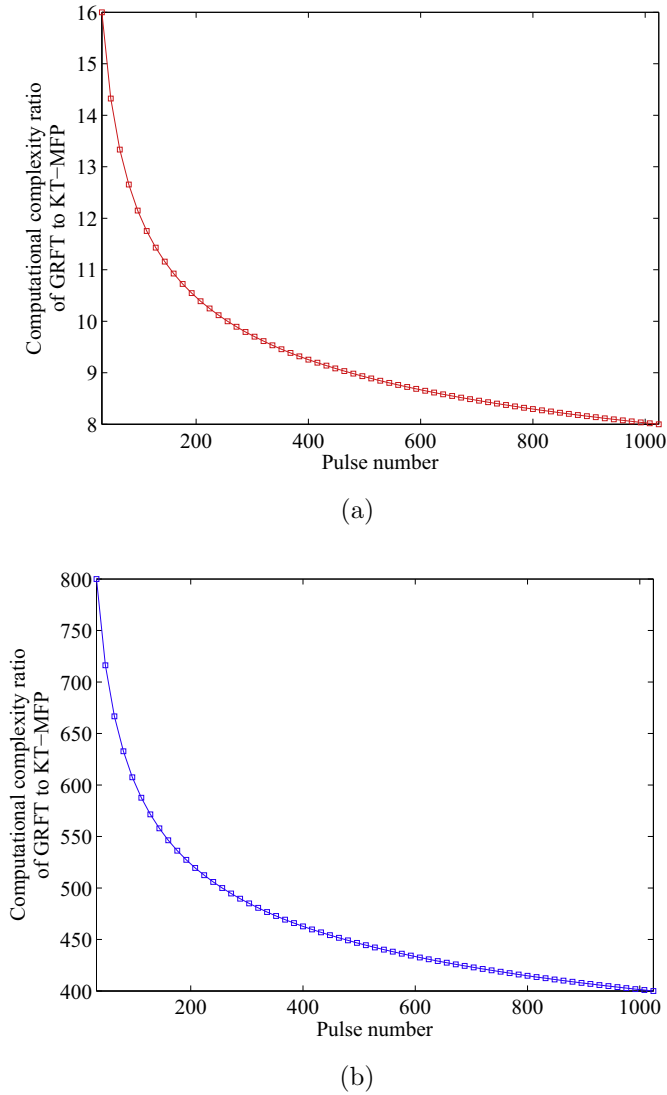


**Fig. 2.** Computational complexity ratio of GRFT to KT-MFP versus the pulse number. (a) Ratio for the low-speed target. (b) Ratio for the high-speed target.

ticular, the computational complexity ratio for the low-speed target is shown in Fig. 2(a). We can see that the computational complexity ratio of GRFT to the proposed method is bigger than 8. As for the computational complexity ratio for the high-speed target in Fig. 2(b), it is larger than 400. Overall, the computational complexity of KT-MFP is lower than the GRFT's.

#### 4. Numerical results

To evaluate the efficiency of the proposed coherent integration method, numerical simulations are provided in this section. In order to carry out the comparison experiment for a single target with low-speed or high-speed, several popular methods, i.e., RFT, IAR-FRFT, KT-FRFT and GRFT are presented. Moreover, the detection performance for the low-speed and high-speed target as well as the coherent integration for multi-targets are also evaluated hereinbelow.

##### 4.1. Coherent integration for a low-speed target

We analyze the coherent integration for a single target with low-speed via KT-MFP in Fig. 3 at first. Note that we use the radar

parameters of Table 2 in this section. Suppose that the motion parameters of the low-speed target as  $r_0 = 200$  km,  $a_1 = 120$  m/s and  $a_2 = 21$  m/s $^2$ , respectively. The signal-to-noise ratio (SNR) after PC is 6 dB. Fig. 3(a) shows the result after the PC, which indicates that serious RM occurs. After applying the KT, Fig. 3(b) shows the jointly searching result of the fold factor and acceleration via MFP. Through the peak value, we can easily find that the estimated acceleration is 21 m/s $^2$  and the estimated fold factor is equivalent to 1. Besides, Fig. 3(c) gives the unambiguous velocity estimation result which is related to  $f_{th}$  and the estimated value is 26.23 m/s. So it is easily to work out the estimated velocity as 119.98 m/s. Fig. 3(d) shows the RM correction result with the estimated motion parameters and it could be seen that all the RM has been removed. After eliminating the effect of RM, the coherent integration result through KT-MFP is shown in Fig. 3(e), from which we can find that the energy is focused and integrated well.

With the purpose of contrast, the coherent integration results of RFT, IAR-FRFT, KT-FRFT and GRFT are also given in Fig. 4. Fig. 4(a)–4(d) show the integration results of the four methods above, respectively. In particular, Fig. 4(a) gives the integration result of RFT and it cannot focus the energy at all because of the DFM induced by target's acceleration. Fig. 4(b) and 4(c) show respectively the integration results of IAR-FRFT and KT-FRFT. We can see that although the target's energy is still accumulated, the integration performance of IAR-FRFT or KT-FRFT will decrease because of the quadratic RM, which will result in detection performance loss compared with KT-MFP (as shown in Section 4.2). Besides, Fig. 4(d) gives the integration result of GRFT which can achieve the coherent integration of target's energy. However, the computational complexity of GRFT is larger than the KT-MFP's.

##### 4.2. Detection performance for a low-speed target

In this section, we compare the detection performance of RFT, IAR-FRFT, KT-FRFT, GRFT and the proposed method for a low-speed target via the Monte Carlo trials. It is necessary to note that we make use of the radar parameters in Table 2 and the same motion parameters in Fig. 3. Subsequently, we set the false alarm probability as  $P_{fa} = 10^{-4}$  and all echoes are submerged in Gaussian noises [47,48]. Fig. 5 shows the detection probabilities of the above-mentioned methods in different SNRs. The SNRs vary from -20 dB to 20 dB. It is clearly that the detection performance of the proposed method precedes KT-FRFT, IAR-FRFT and RFT. Because of the sinc-like interpolation of the KT, the proposed method suffers slight performance loss, in comparison with GRFT. However, KT-MFP requires lower computational cost than GRFT.

##### 4.3. Coherent integration for a high-speed target

In the following simulation, we assess the coherent integration for a high-speed target via the proposed method in Fig. 6. The simulation parameters of radar in this section is listed in Table 3. The motion parameters of the high-speed target are  $r_0 = 500$  km,  $a_1 = 3000.8$  m/s and  $a_2 = 310$  m/s $^2$ . Here we also set the SNR after PC as 6 dB. According to Fig. 6(a), we could see that serious RM happens after the PC. Fig. 6(b) shows the jointly searching result of the fold factor and acceleration after applying KT and MFP. The peak value denotes that the estimated acceleration is equal to 310 m/s $^2$  and the estimated fold factor is 1000. Fig. 6(c) gives the unambiguous velocity estimation result is 0.81 m/s. So the estimated velocity is equal to 3000.81 m/s. Fig. 6(d) shows that RM has been corrected using the estimated motion parameters. After eliminating the effect of RM, the coherent integration result through KT-MFP is given in Fig. 6(e) where the energy of the high-speed target is also integrated well.

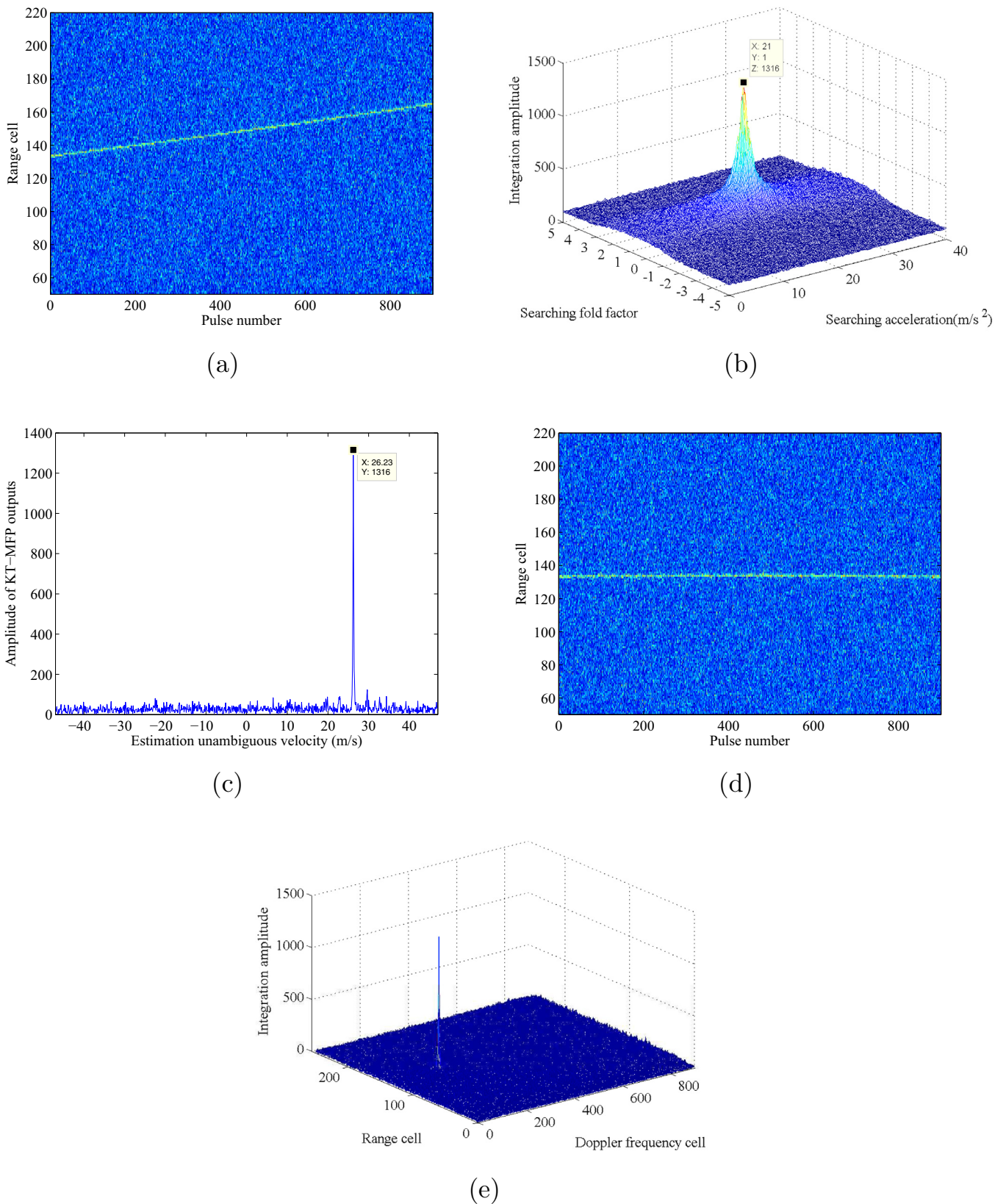


**Fig. 3.** Coherent integration for a low-speed target via KT-MFP. (a) Result after PC. (b) Jointly searching result of the fold factor and acceleration. (c) Estimation result of unambiguous velocity. (d) RM correction result. (e) Integration result of KT-MFP.

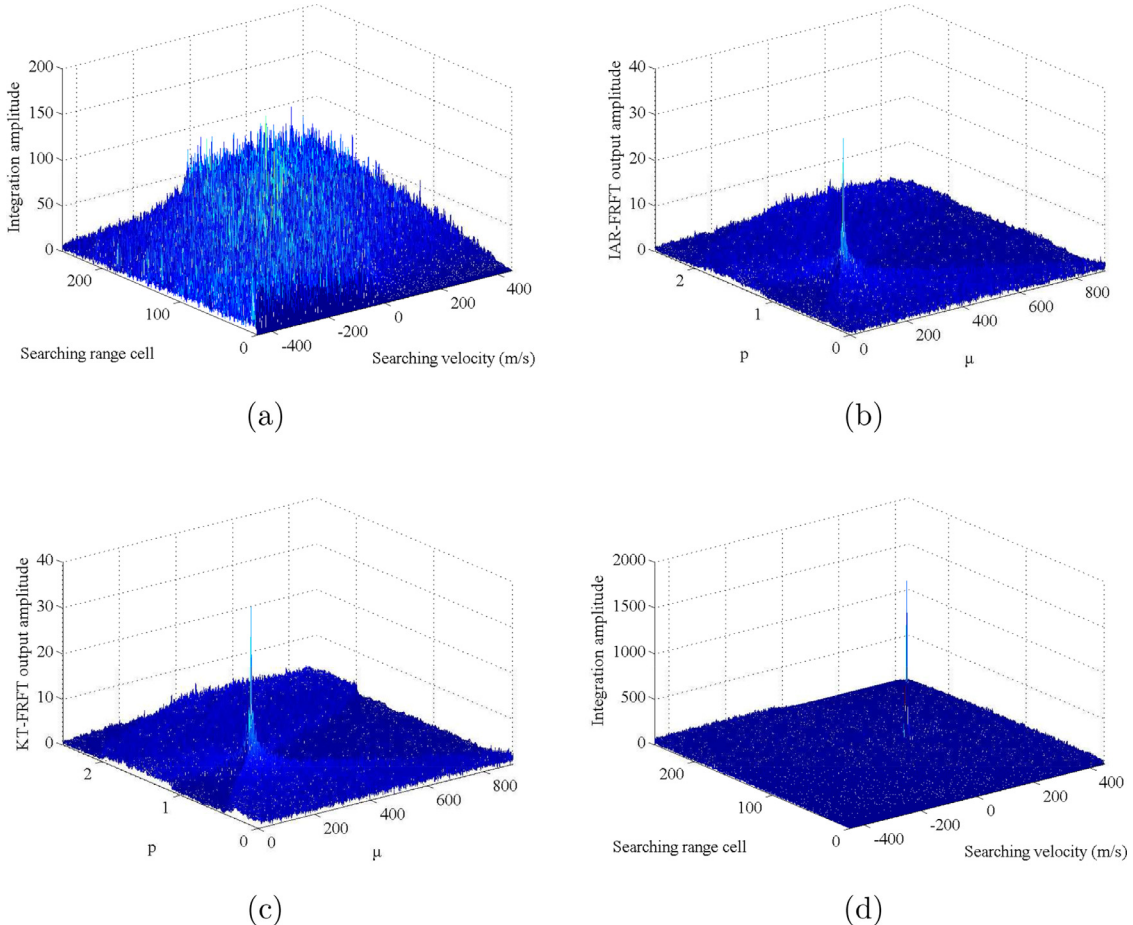


**Fig. 4.** Coherent integration for a low-speed target via RFT, IAR-FRFT, KT-FRFT and GRFT. (a) Integration result of RFT. (b) Integration result of IAR-FRFT. (c) Integration result of KT-FRFT. (d) Integration result of GRFT.

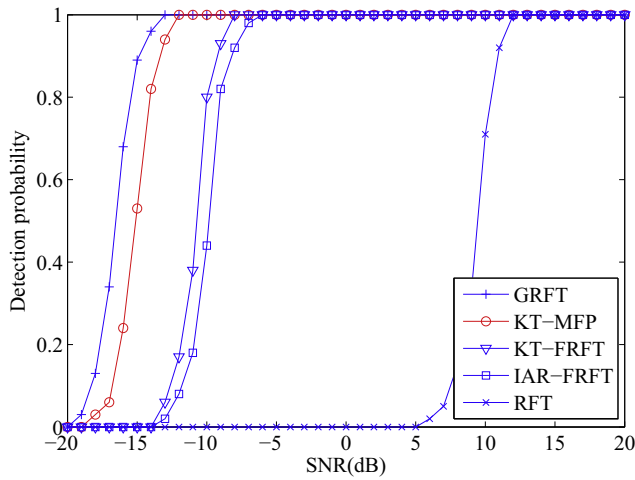


**Fig. 5.** Detection probability of RFT, IAR-FRFT, KT-FRFT, GRFT and KT-MFP for a low-speed target.

In order to make a comparison, the coherent integration performance of other popular methods, i.e., RFT, IAR-FRFT, KT-FRFT and GRFT, is also shown in Fig. 7. Fig. 7(a)–7(d) show the integration results of the aforementioned methods, respectively. Specifically, Fig. 7(a) shows that RFT cannot accumulate the energy mainly because of the DFM effect caused by target's acceleration. Moreover, Fig. 7(b) and 7(c) show respectively the integration results of IAR-

FRFT and KT-FRFT. Because of target's high speed and the high radar carrier frequency, the undersampling along the slow time dimension would occur and then the FRFT-based integration methods (i.e., IAR-FRFT and KT-FRFT) will become invalid. Furthermore, Fig. 7(d) gives the integration result of the GRFT method. Although GRFT also could obtain the coherent integration, there appears the BSSL effect in the GRFT output, which might bring about severe false alarm and reduce the multi-targets detection ability.

#### 4.4. Detection performance for a high-speed target

We compare the detection performance of RFT, IAR-FRFT, KT-FRFT, GRFT and KT-MFP for a high-speed target in this simulation, where the Monte Carlo trials are performed. One should point out that we still use the radar parameters in Table 3 and the motion parameters are identical to those in Fig. 6. The false alarm probability is set as  $P_{fa} = 10^{-4}$  and the Gaussian noises are added to the target's echoes. Fig. 8 shows the detection probabilities of the KT-MFP method with other four methods in different SNR cases. The SNRs also vary in [-20 dB, 20 dB]. One could clearly see that the detection performance of KT-MFP is far better than that of KT-FRFT, IAR-FRFT and RFT. In fact, the undersampling of the slow time might appear on account of target's high speed and radar's high carrier frequency, so IAR-FRFT and KT-FRFT would become invalid and their detection performance decrease a lot. Although the detection performance of the proposed method declines slightly (still because of the sinc-like interpolation for KT) compared with GRFT, the KT-MFP method has lower computational cost without the BSSL effect.

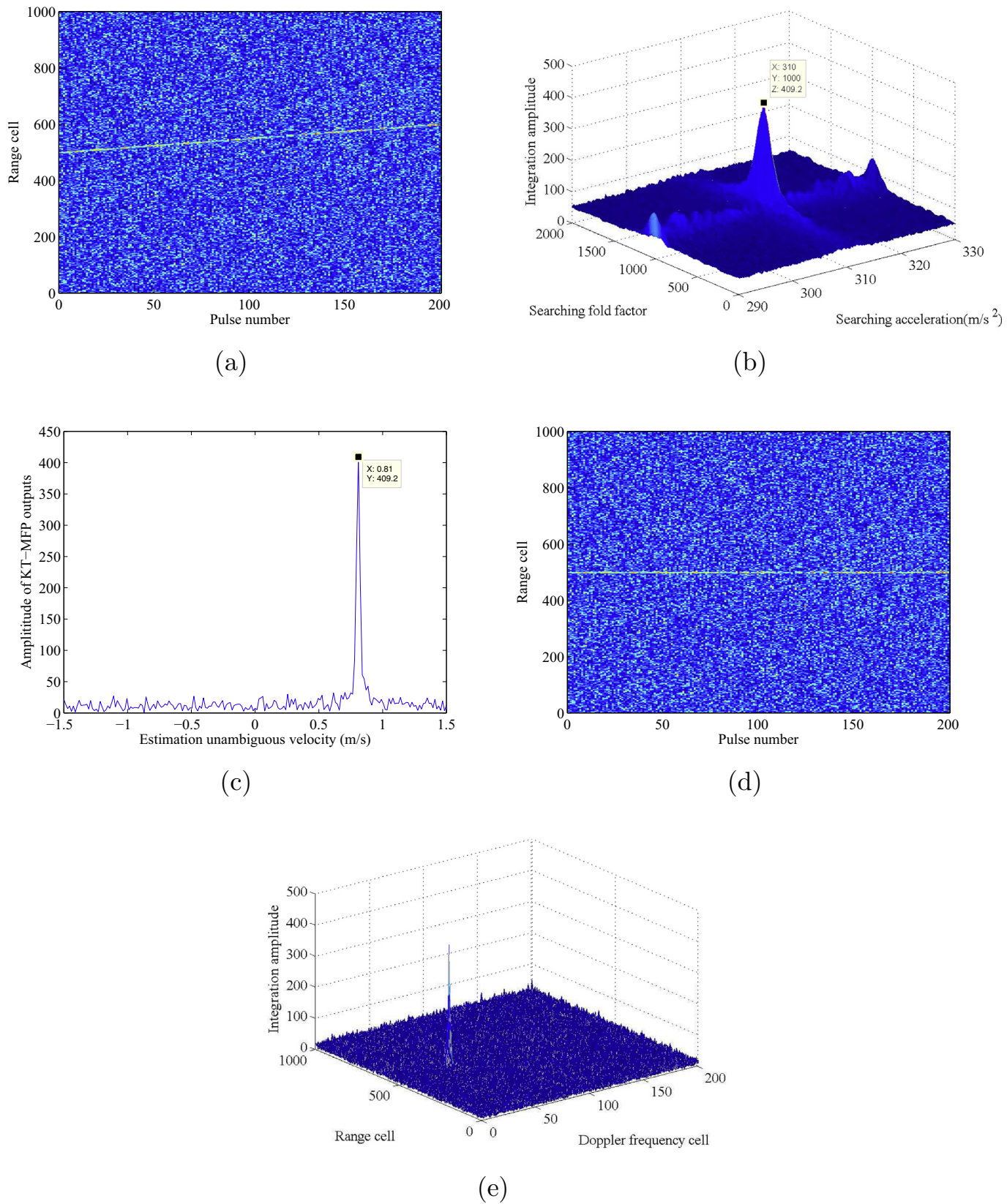


**Fig. 6.** Coherent integration for a high-speed target via KT-MFP. (a) Result after PC. (b) Jointly searching result of the fold factor and acceleration. (c) Estimation result of unambiguous velocity. (d) RM correction result. (e) Integration result of KT-MFP.

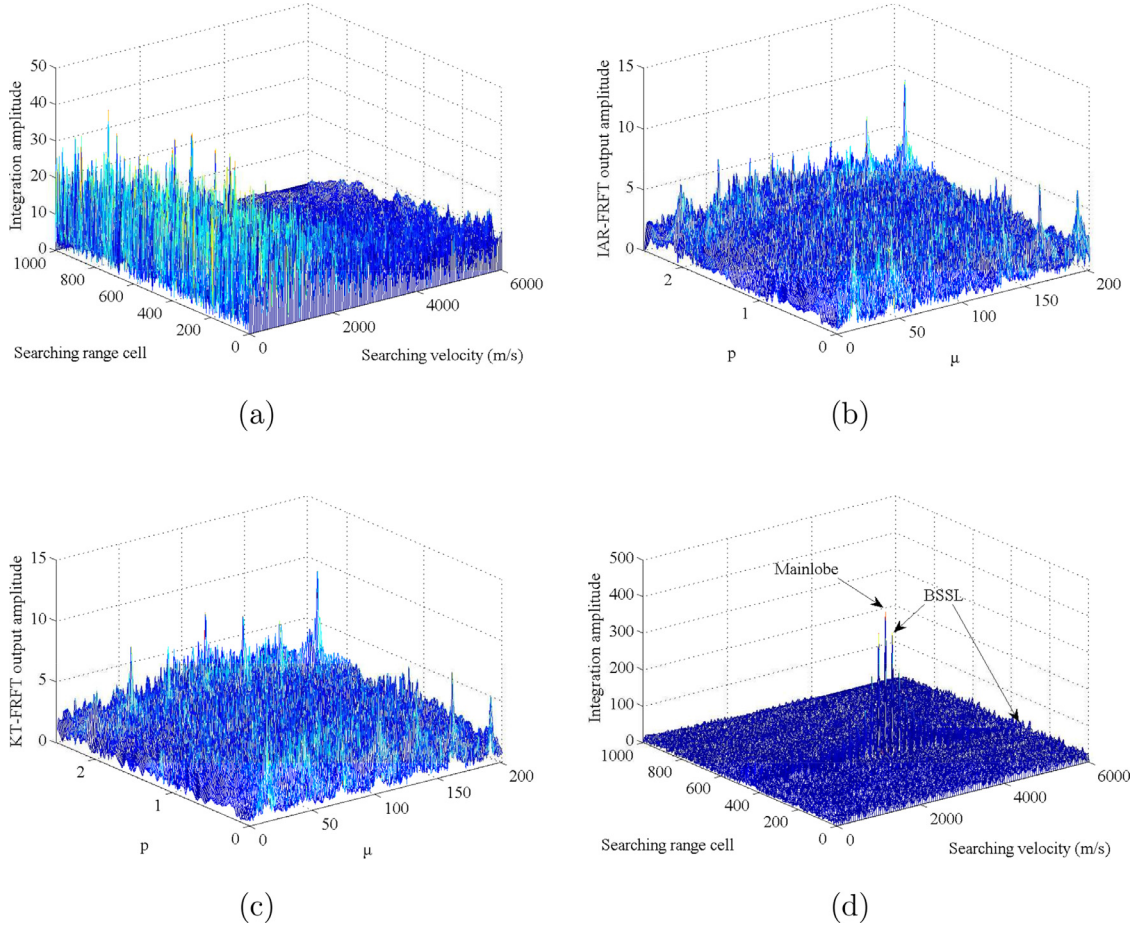


**Fig. 7.** Coherent integration for a high-speed target via RFT, IAR-FRFT, KT-FRFT and GRFT. (a) Integration result of RFT. (b) Integration result of IAR-FRFT. (c) Integration result of KT-FRFT. (d) Integration result of GRFT.

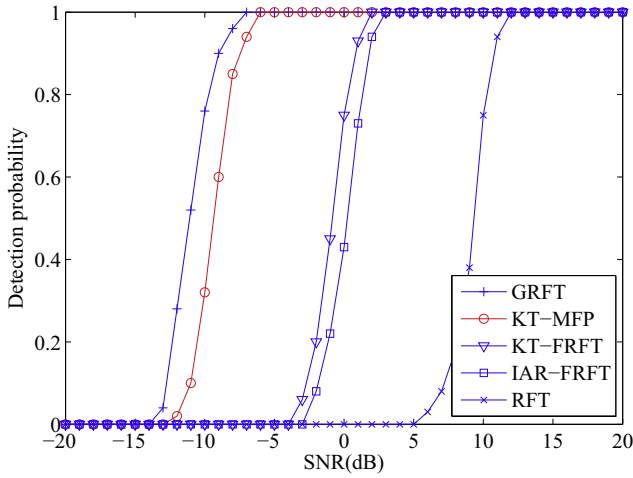


**Fig. 8.** Detection probability of RFT, IAR-FRFT, KT-FRFT, GRFT and KT-MFP for a high-speed target.

#### 4.5. Coherent integration for multiple targets

In this section, we evaluate the coherent integration ability of KT-MFP for multiple targets and the motion parameters of target A and B are listed in Table 4. The radar parameters are given in Table 2 and the SNRs (after PC) of the two targets are both 6 dB. The simulation results of KT-MFP for multiple targets are

**Table 4**  
Motion parameters of two moving targets.

Motion parameters	Target A	Target B
Initial slant range	180 km	220 km
Radial velocity	80 m/s	-100 m/s
Radial acceleration	20 m/s <sup>2</sup>	-15 m/s <sup>2</sup>
SNR(after PC)	6 dB	6 dB

given in Fig. 9. Particularly, Fig. 9(a) shows the result after the PC while Fig. 9(b) gives the jointly searching result of fold factors and accelerations. Specifically, the estimated fold factors are 1 and -1 for the two targets, separately. Besides, according to the peak values, the estimated accelerations are 20 m/s<sup>2</sup> and -15 m/s<sup>2</sup>. Fig. 9(c) gives the estimation result of unambiguous velocities. As for target A, the estimated unambiguous velocity is -13.82 m/s and then we can work out that the estimation of target A's velocity is 79.93 m/s. In terms of target B, the estimated unambiguous velocity is -6.31 m/s and the estimated velocity is equal to -100.06 m/s. Furthermore, Fig. 9(d) gives the coherent integration result via the proposed method and we can see that the energy of the two targets is well focused. It should be noted that if the scattering intensities of different targets differ significantly, we can use the CLEAN technique to realize the coherent integration (as analyzed in Section 3.3). Finally, we can conclude that KT-MFP is also effective for the coherent integration of multiple targets.

Overall, for the low-speed target, the proposed method could eliminate the RM and DFM effectively to integrate the energy well.

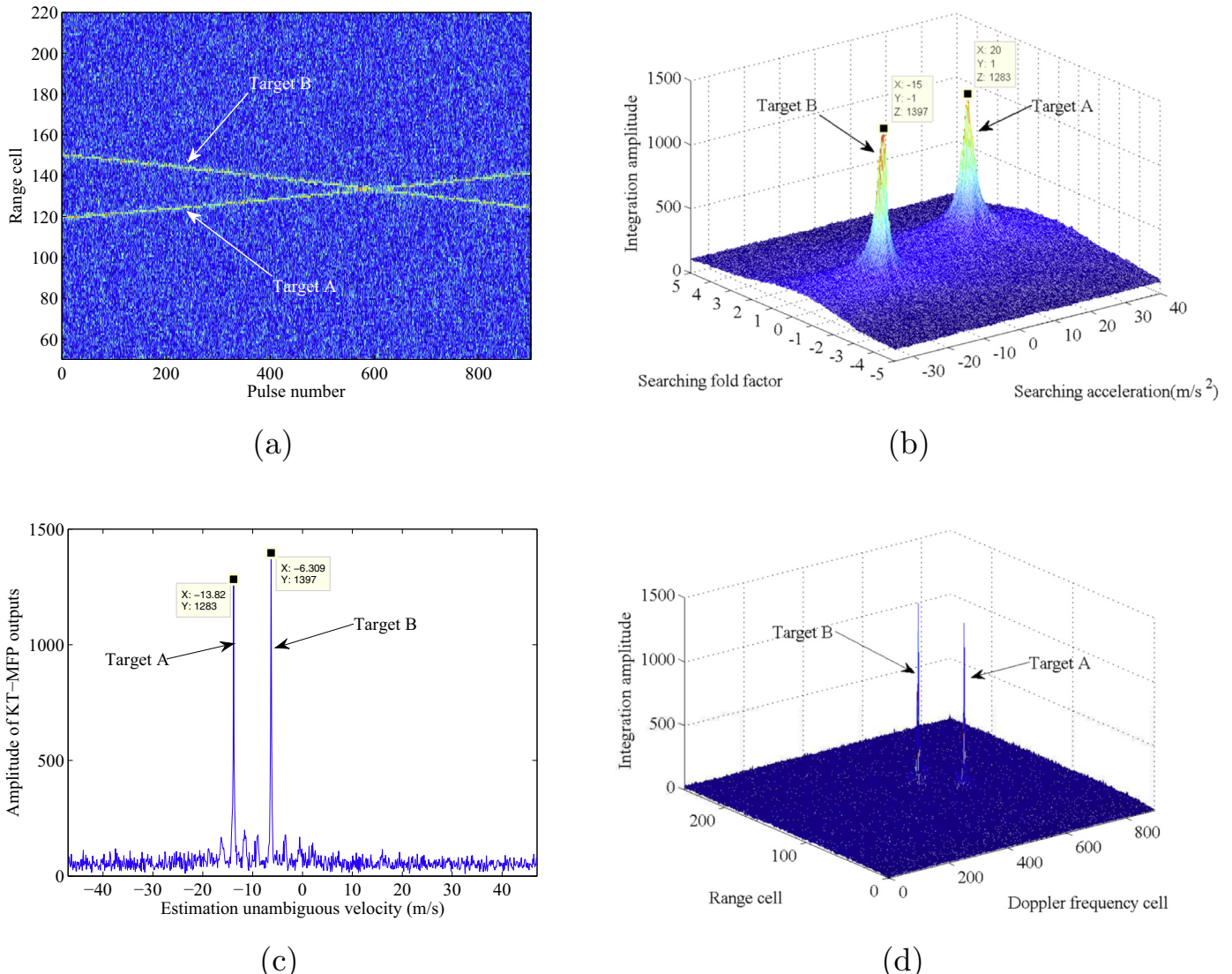


**Fig. 9.** Coherent integration for multiple targets via the proposed method. (a) Result after PC. (b) Jointly searching result of the fold factors and accelerations. (c) Estimation result of unambiguous velocities. (d) Integration result via the proposed method.

Moreover, it has a better detection performance than RFT, IAR-FRFT and KT-FRFT. Although there is a slight loss for the detection performance compared with GRFT, the proposed method has lower computational cost. While in terms of the coherent integration for a high-speed target, the proposed algorithm can still perform well to accumulate the energy when RFT, IAR-FRFT and KT-FRFT all become invalid and there appears the BSSL effect for the GRFT method. Additionally, the last simulation has validated the coherent integration ability of KT-MFP for multiple targets.

## 5. Conclusion

In this paper, we have presented a new method named KT-MFP for the weak maneuvering target detection. The KT-MFP method can both eliminate the RM and DFM effects within the coherent pulse interval. In particular, this method firstly corrects the linear RM resulted from the unambiguous velocity via KT and then performs the MFP in the range frequency-slow time domain to eliminate the residual RM (including the residual linear RM caused by the blind velocity and the quadratic RM resulted from the acceleration) and the DFM. Finally, coherent integration of the target's

energy is achieved via the slow time FT. The simulations about the coherent integration ability and detection performance have been carried out in detail. In general, the results show that the KT-MFP method is able to perform well whether for the low-speed target or the high-speed target and could avoid the BSSL effect but requires lower computational complexity compared with GRFT. In addition, the detection performance of KT-MFP outperforms that of RFT, IAR-FRFT and KT-FRFT.

## Acknowledgments

This work was supported by the Chang Jiang Scholars Program, the Fundamental Research Funds of Central Universities under Grants ZYGX2016J031, the Chinese Postdoctoral Science Foundation under Grant 2014M550465 and Special Grant 2016T90845.

## References

- [1] J. Yu, J. Xu, Y.N. Peng, X.G. Xia, Radon-Fourier transform (RFT) for radar target detection (III): optimality and fast implementations, *IEEE Trans. Aerosp. Electron. Syst.* 48 (2) (2012) 991–1004.

- [2] X.L. Li, G.L. Cui, W. Yi, L.J. Kong, A fast maneuvering target motion parameters estimation algorithm based on ACCF, *IEEE Signal Process. Lett.* 22 (3) (2015) 270–274.
- [3] S.Q. Zhu, G.S. Liao, D. Yang, H.H. Tao, A new method for radar high-speed maneuvering weak target detection and imaging, *IEEE Geosci. Remote Sens. Lett.* 11 (7) (2014) 1175–1179.
- [4] J. Su, M. Xing, G. Wang, Z. Bao, High-speed multi-target detection with narrowband radar, *IET Radar Sonar Navig.* 4 (4) (2010) 595–603.
- [5] M.D. Xing, J.H. Su, G.Y. Wang, Z. Bao, New parameter estimation and detection algorithm for high speed small target, *IEEE Trans. Aerosp. Electron. Syst.* 47 (1) (2011) 214–224.
- [6] J. Tian, W. Cui, S.L. Wu, A novel method for parameter estimation of space moving targets, *IEEE Geosci. Remote Sens. Lett.* 11 (2) (2014) 389–393.
- [7] L.C. Qian, J. Xu, X.G. Xia, W.F. Sun, T. Long, Y.N. Peng, Fast implementation of generalized radon-fourier transform for manoeuvring radar target detection, *Electron. Lett.* 48 (22) (2012) 1427–1428.
- [8] G.H. Zhao, Z.Y. Wang, Q. Wang, G.M. Shi, F.F. Shen, Robust ISAR imaging based on compressive sensing from noisy measurements, *Signal Process.* 92 (1) (2012) 120–129.
- [9] C. Sun, B.P. Wang, Y. Fang, K.F. Yang, Z.X. Song, High-resolution ISAR imaging of maneuvering targets based on sparse reconstruction, *Signal Process.* 108 (2015) 535–548.
- [10] X. Rao, H.T. Huang, J. Xie, J. Su, W.P. Li, Long-time coherent integration detection of weak manoeuvring target via integration algorithm, improved axis rotation discrete chirp-Fourier transform, *IET Radar Sonar Navig.* 9 (7) (2015) 917–926.
- [11] X.L. Chen, J. Guan, N.B. Liu, Y. He, Maneuvering target detection via Radon-Fractional Fourier transform-based long-time coherent integration, *IEEE Trans. Signal Process.* 62 (4) (2014) 939–953.
- [12] X.L. Chen, J. Guan, Z.H. Bao, Y. He, Detection and extraction of target with micro-motion in spiky sea clutter via short-time fractional fourier transform, *IEEE Trans. Geosci. Remote Sens.* 52 (2) (2014) 1002–1018.
- [13] S.B. Peng, J. Xu, X.G. Xia, F. Liu, T. Long, J. Yang, Y.N. Peng, Multiaircraft formation identification for narrowband coherent radar in a long coherent integration time, *IEEE Trans. Aerosp. Electron. Syst.* 51 (3) (2015) 2121–2136.
- [14] X.L. Li, G.L. Cui, W. Yi, L.J. Kong, Coherent integration for maneuvering target detection based on Radon-Lv's distribution, *IEEE Signal Process. Lett.* 22 (9) (2015) 1467–1471.
- [15] X.L. Li, G.L. Cui, W. Yi, L.J. Kong, Radar maneuvering target detection and motion parameter estimation based on TRT-SGRFT, *Signal Process.* 133 (2017) 107–116.
- [16] P.H. Huang, G.S. Liao, Z.W. Yang, J.T. Ma, An approach for refocusing of ground fast-moving target and high-order motion parameter estimation using Radon-high-order time-chirp rate transform, *Digital Signal Process.* 48 (2016) 333–348.
- [17] C.S. Pang, S. Tao, R. Tao, N. Zhang, Detection of high-speed and accelerated target based on the linear frequency modulation radar, *IET Radar Sonar Navig.* 8 (1) (2014) 37–47.
- [18] R. Tao, N. Zhang, Y. Wang, Analysing and compensating the effects of range and doppler frequency migrations in linear frequency modulation pulse compression radar, *IET Radar Sonar Navig.* 5 (1) (2011) 12–22.
- [19] X.L. Li, G.L. Cui, W. Yi, L.J. Kong, Manoeuvring target detection based on keystone transform and Lv's distribution, *IET Radar Sonar Navig.* 10 (7) (2016) 1234–1242.
- [20] J. Xu, Y.N. Peng, X.G. Xia, T. Long, E.K. Mao, A. Farina, Focus-before-detection radar signal processing (I): challenges and methods, accepted for publication in IEEE aerospace and electronic systems magazine.
- [21] J. Xu, Y.N. Peng, X.G. Xia, T. Long, E.K. Mao, A. Farina, Focus-before-detection radar signal processing (II): recent developments, accepted for publication in IEEE aerospace and electronic systems magazine.
- [22] R.P. Perry, R.C. Dipietro, R.L. Fante, *SAR Imaging of moving targets*, *IEEE Trans. Aerosp. Electron. Systems* 35 (1) (1999) 188–200.
- [23] D.Y. Zhu, Y. Li, Z.D. Zhu, A keystone transform without interpolation for SAR ground moving-target imaging, *IEEE Geosci. Remote Sens. Lett.* 4 (1) (2007) 18–22.
- [24] S.J. Yuan, T. Wu, M. Mao, G.J. Mei, X. Wei, Application research of keystone transform in weak high-speed target detection in low-PRF narrowband chirp radar, in: *Proceedings of 2008 9th International Conference on Signal Processing*, Beijing, China, 2008, pp. 2452–2456.
- [25] G. Li, X.G. Xia, Y.N. Peng, Doppler keystone transform: an approach suitable for parallel implementation of SAR moving target imaging, *IEEE Geosci. Remote Sens. Lett.* 5 (4) (2008) 573–577.
- [26] J. Xu, J. Yu, Y.N. Peng, X.G. Xia, Radon-Fourier transform (RFT) for radar target detection (I): generalized Doppler filter bank processing, *IEEE Trans. Aerosp. Electron. Syst.* 47 (2) (2011) 1186–1202.
- [27] J. Xu, J. Yu, Y.N. Peng, X.G. Xia, Radon-Fourier transform (RFT) for radar target detection (II): blind speed sidelobe suppression, *IEEE Trans. Aerosp. Electron. Syst.* 47 (4) (2011) 2473–2489.
- [28] X.L. Li, G.L. Cui, W. Yi, L.J. Kong, An efficient integration method for maneuvering target detection, in: *2015 IET International Radar Conference*, 2015, pp. 1–6.
- [29] X. Rao, H.H. Tao, J. Su, J. Xie, X.Y. Zhang, Detection of cosntant radial acceleration weak target via IAR-FRFT, *IEEE Trans. Aerosp. Electron. Syst.* 51 (4) (2015) 3242–3253.
- [30] J. Xu, X.G. Xia, S.B. Peng, J. Yu, Y.N. Peng, L.C. Qian, Radar maneuvering target motion estimation based on generalized radon-fourier transform, *IEEE Trans. Signal Process.* 60 (12) (2012) 6190–6201.
- [31] X.L. Li, L.J. Kong, G.L. Cui, W. Yi, A low complexity coherent integration method for maneuvering target detection, *Digital Signal Process.* 49 (2016) 137–147.
- [32] X.L. Chen, J. Guan, Y. Huang, N.B. Liu, Y. He, Radon-linear canonical ambiguity function-based detection and estimation method for marine target with micro-motion, *IEEE Trans. Geosci. Remote Sens.* 53 (4) (2015) 2225–2240.
- [33] P.H. Huang, G.S. Liao, Z.W. Yang, X.G. Xia, A fast SAR imaging method for ground moving target using a second-order WVD transform, *IEEE Trans. Geosci. Remote Sens.* 54 (4) (2016) 1940–1956.
- [34] Y. Wang, Y.C. Jiang, ISAR imaging of maneuvering target based on the L-Class of fourth-order complex-lag PWVD, *IEEE Trans. Geosci. Remote Sens.* 48 (3) (2010) 1518–1527.
- [35] Y. Wang, Y.C. Jiang, Inverse synthetic aperture radar imaging of maneuvering target based on the product generalized cubic phase function, *IEEE Geosci. Remote Sens. Lett.* 8 (5) (2011) 958–962.
- [36] Y.C. Li, M.D. Xing, Y.H. Quan, Z. Bao, A new algorithm of ISAR imaging for maneuvering targets with low SNR, *IEEE Trans. Aerosp. Electron. Syst.* 49 (1) (2013) 543–557.
- [37] J.B. Zheng, T. Su, W.T. Zhu, Q.H. Liu, ISAR imaging of targets with complex motions based on the keystone time-chirp rate distribution, *IEEE Geosci. Remote Sens. Lett.* 11 (7) (2014) 1275–1279.
- [38] J.B. Zheng, T. Su, L. Zhang, W.T. Zhu, Q.H. Liu, ISAR imaging of targets with complex motion based on the chirp rate-quadratic chirp rate distribution, *IEEE Trans. Geosci. Remote Sens.* 52 (11) (2014) 7276–7289.
- [39] M.R. Sharif, S.S. Abeysekera, Efficient wideband signal parameter estimation using a single slice of radon-ambiguity transform, in: *Proceedings of IEEE International Conference on Acoustics, Speech and Signal Processing*, 5, 2005, pp. 605–608.
- [40] M.R. Sharif, S.S. Abeysekera, Efficient wideband signal parameter estimation using a Radon-ambiguity transform slice, *IEEE Trans. Aerosp. Electron. Syst.* 43 (2) (2007) 673–688.
- [41] G.C. Sun, M.D. Xing, X.G. Xia, Y.R. Wu, Z. Bao, Robust ground moving-target imaging using Deramp-keystone processing, *IEEE Trans. Geosci. Remote Sens.* 51 (2) (2013) 966–982.
- [42] J. Tian, W. Cui, X.G. Xia, S.L. Wu, Parameter estimation of ground moving targets based on SKT-DLVT processing, *IEEE Trans. Comput. Imaging* 2 (1) (2016) 13–26.
- [43] P.H. Huang, G.S. Liao, Z.W. Yang, X.G. Xia, Long-time coherent integration for weak maneuvering target detection and high-order motion parameter estimation based on keystone transform, *IEEE Trans. Signal Process.* 64 (15) (2016) 4013–4026.
- [44] X.L. Li, L.J. Kong, G.L. Cui, W. Yi, CLEAN-based coherent integration method for high-speed multi-targets detection, *IET Radar Sonar Navig.* 10 (9) (2016) 1671–1682.
- [45] J. Misiurewicz, K.S. Kulpa, Z. Czekala, T.A. Filipek, Radar detection of helicopters with application of CLEAN method, *IEEE Trans. Aerosp. Electron. Syst.* 48 (4) (2012) 3525–3537.
- [46] Q. Wang, M.D. Xing, G.Y. Lu, Z. Bao, SRMF-CLEAN imaging algorithm for space debris, *IEEE Trans. Antennas Propag.* 55 (12) (2007) 3524–3533.
- [47] L.J. Kong, X.L. Li, G.L. Cui, W. Yi, Y.C. Yang, Coherent integration algorithm for a maneuvering target with high-order range migration, *IEEE Trans. Signal Process.* 63 (17) (2015) 4474–4486.
- [48] X.L. Li, G.L. Cui, L.J. Kong, W. Yi, Fast non-searching method for maneuvering target detection and motion parameters estimation, *IEEE Trans. Signal Process.* 64 (9) (2016) 2232–2244.